Journal of Fluids and Structures 17 (2003) 833–853

JOURNAL OF FLUIDS AND STRUCTURES

www.elsevier.nl/locate/jnlabr/yjfls

Influence of an unvented tunnel entrance hood on the compression wave generated by a high-speed train

M.S. Howe[a,*], M. Iida[b], T. Fukuda[b]

[a] *College of Engineering, Boston University, 110 Cummington Street, Boston, MA 02215, USA*
[b] *Railway Technical Research Institute, 2-8-38 Hikari-cho, Kokubunji-shi, Tokyo 185-8540, Japan*

Received 7 September 2001; received in revised form 29 April 2002; accepted 19 July 2002

Abstract

A theoretical and experimental study is made of the compression wave generated when a train enters a nominally uniform tunnel with a long, unvented entrance hood. The purpose of the hood is to reduce as much as practicable the maximum gradient of the compression wave front. The pressure gradient can increase in a long tunnel as a result of nonlinear wave steepening, and thereby increase the impact on residential dwellings of the acoustic 'boom' (or *micro-pressure wave*) radiated from the far end of the tunnel when the compression wave arrives. Our experiments are conducted at model scale using axisymmetric 'trains' projected at speeds up to 350 kph along the axis of a cylindrical tunnel fitted with a cylindrical entrance hood. Theoretical predictions of the compression wave are made using the equation of aerodynamic sound containing a slender body approximation to the effective source representing the moving train, coupled with a small correction that accounts for the 'vortex' sources in the free shear layers in the exit flows from the hood and tunnel of the air displaced by the train. The compression wave is generated by the two successive interactions of the train nose with the hood portal and with the junction between the hood and tunnel. The interactions produce a system of compression and expansion waves, each having characteristic wavelengths that are much smaller than the hood length; the waves are temporarily reflected back and forth within the hood prior to transmission into the tunnel, and are resolved analytically by use of an approximate Green's function determined by the hood geometry. Theoretical predictions are found to be in excellent agreement with experiment, including in particular a detailed correspondence between measured and predicted interference patterns produced by the multiple reflections of waves in the hood.

1. Introduction

A train entering a tunnel generates a compression wave that propagates ahead of the train at the speed of sound (Hara, 1961; Hara et al., 1968; Ozawa et al., 1976, Ozawa and Maeda, 1988a, 1991; Woods and Pope, 1976). The pressure rise across the wavefront is given approximately by

$$\Delta p = \frac{\rho_o U^2}{(1-M^2)}\frac{\mathscr{A}_o}{\mathscr{A}}\left(1+\frac{\mathscr{A}_o}{\mathscr{A}}\right), \tag{1.1}$$

where ρ_o, U, $\mathscr{A}_o$ and $\mathscr{A}$, respectively, denote the mean air density, train speed, and the cross-sectional areas of the train and the uniform section of the tunnel, and $M = U/c_o$ is the train Mach number and c_o the speed of sound (Howe et al., 2000). Modern high-speed 'intercity' trains generally travel at speeds $U > 200$ kph and the tunnel 'blockage'

*Corresponding author. Tel.: +1-617-484-0656; fax: +1-617-353-5866.
E-mail address: mshowe@bu.edu (M.S. Howe).

0889-9746/03/$ - see front matter
doi:10.1016/S0889-9746(03)00011-2

$\mathscr{A}_o/\mathscr{A} \sim 0.15$–$0.2$, so that Δp is typically about 1–3% of atmospheric pressure. A rarefaction wave of equal amplitude is generated as the tail of the train enters the tunnel. Complex pressure patterns develop within the tunnel by multiple reflections from the tunnel exits and other geometric discontinuities, and constructive interference occurring at very high operating speeds can produce large overpressures.

When the compression wave is reflected from the distant tunnel exit a pressure pulse, called the *micro-pressure wave*, is radiated out of the tunnel. The strength of this pulse is proportional to the wavefront steepness of the compression wave. The initial profile of the wavefront just after the entry of the train into the tunnel is determined principally by the shape of the tunnel entrance portal, the train noise profile, and the blockage $\mathscr{A}_o/\mathscr{A}$ (Maeda et al., 1993; Ogawa and Fujii, 1994, 1997; Iida et al., 1996; Noguchi et al., 1996; Gregoire et al., 1997; Matsuo et al., 1997; Howe, 1998a, b, 1999; Ito, 2000; Peters, 2000). When $\mathscr{A}_o/\mathscr{A}$ is small and the portal is unmodified with mean radius R (i.e., the radius of the circle whose area equals the cross-sectional area of the tunnel), the compression wavefront is generated over a time of order R/U, and therefore the initial wavefront thickness $\sim R/M \gg R$. However, many of the newer long tunnels (longer than about 3 km, say) are fitted with maintenance-free and 'acoustically smooth' concrete slab tracks that tend to promote nonlinear steepening of the compression wave as it propagates in the tunnel. This greatly increases the micro-pressure wave amplitude, making it comparable in strength to a sonic boom from a supersonic aircraft, and producing unsettling structural vibrations in neighbouring buildings. At higher train speeds the wave is perceived as a loud 'bang', whose incidence constitutes a serious impediment to proposed speed increases in urban areas (up to 500 kph, or so, for *Maglev* trains), particularly as new high-speed routes are expected to involve many long tunnels accounting for 50% or more of a journey.

Ozawa et al. (1991) pointed out that nonlinear steepening in a long tunnel tends to be inhibited by diffusive wave thickening produced by dissipation, provided the *initial* thickness of the compression wave is sufficiently large (see also Maeda et al., 1993; Iida et al., 1996). Wave energy is dissipated in tunnels with conventional ballasted track by frictional losses produced by air penetration into ballast. In Japan, however, most high-speed railway tunnels are slab-tracked, without dissipative cavities, and there is great interest in alternative means of avoiding nonlinear steepening by greatly increasing the initial 'rise time' of the compression wave by novel tunnel portal design (a review of these alternative methods is given by Ozawa et al., 1991). The most widely used portal modification consists of installing a tunnel entrance 'hood', which is a cylindrical thin-walled structure extending up to 50 m ahead of the tunnel entrance. A hood usually has 'windows' in the sidewalls or roof, judiciously distributed to allow the progressive venting to the atmosphere of high-pressure air produced by an entering train, thereby increasing the width of the compression wavefront.

Early model scale experiments and field measurements made by Ozawa et al. (1978) at speeds $U < 200$ kph ($M < 0.16$) used relatively short hoods of length $\ell_h \sim 3R$. For an unvented hood of radius $> R$ they found that the compression wave profile rises in two steps, the first produced when the train enters the hood and the second when the train passes from the hood into the tunnel (see, also, the recent measurements of Sasoh et al., 1994), and that the maximum pressure gradient can be decreased to about 50% of its value in the absence of the hood by optimizing the cross-sectional area ratio of the hood and tunnel. A further decrease in the maximum pressure gradient, to about 40% of its value with no hood, can be achieved by opening a suitably sized window halfway along the hood and reducing slightly the area ratio from the unvented optimal value. To obtain a significant increase in the compression wave rise time at higher train speeds it is necessary to use longer hoods, and have several windows distributed along the hood at intervals $\sim R$ (Ozawa and Maeda, 1988b, 1991). The longest in current use (at the eastern entrance to the Ohirayama tunnel in Japan) has $\ell_h = 49$ m ($\sim 8R$), and yields a fivefold increase in wave thickness (Ozawa et al., 1991).

An ideal hood would produce a *linear* increase in pressure with distance across the wavefront, with a constant pressure gradient that is as small as practicable. Nonlinear steepening would be inhibited, and there would be a reduced tendency for high-frequency 'shocklets' to form on an otherwise extended, but roughened wavefront. However, at the higher operating speeds of newer trains it is expected that greatly increased hood lengths will be necessary (greater than about $10R$), and the trial and error procedures (based on experiment and numerical simulations) that have hitherto sufficed in hood design will become ineffective. Howe et al. (2000) have demonstrated that a 'flared' entrance hood without windows (whose cross-sectional area varies smoothly and in a prescribed manner with distance from the entrance) can, in principle, behave in the desired manner, but possibly only at greatly increased construction costs and space requirements. A less costly approximation to this optimum can be achieved using a long unvented hood of constant radius $> R$ and relaxing the requirement that the initial wavefront profile be 'smooth'; in this case the profile will be extended and 'wavy', being formed by a superposition of compression and rarefaction waves generated at the ends of the hood, each of wavelength small compared to the overall hood length. Once this optimum has been established further smoothing of the pressure rise should be possible by suitably distributing small vents along the hood.

In this paper we consider the first of these problems, of measuring and predicting the compression wave profile produced when a high-speed train enters a *long*, unvented hood of constant cross-section. When the growth of the turbulent boundary layer on the train within the tunnel and the vorticity in the exit flow from the tunnel portal are both

ignored, the net pressure rise across the wavefront is given by Eq. (1.1) independently of the cross-section of the hood, where $\mathscr{A}$ is the uniform tunnel cross-sectional area (Howe et al., 2000). In a long hood, however, compression waves are generated when the train nose enters and leaves the hood, and multiple reflections cause the temporary confinement of waves within the hood. An analytical representation of wave generation including these effects is given in this paper as an extension of the theory of Howe et al. (2000). However, whereas in the earlier work it could be assumed that the hood length was 'acoustically compact' (the compression wave thickness exceeding ℓ_h), this condition is not satisfied in a long uniform hood, where the compression wave components generated at the ends of the hood have wavelengths $\sim R/M$ that tend to be much shorter than ℓ_h. Our results are compared with model scale experiments, and the theory is shown to supply a clear picture of the various physical interactions involved in the formation of the measured compression wave profiles. The analytical approach permits the influences of tunnel geometry and train nose shape to be evaluated separately, and overall predictions can be made in a matter of minutes (as opposed to the several hours typically required for a numerical integration of the three-dimensional equations of motion, cf. Yoon and Lee, 2001).

The theory of compression wave formation in a long hood is discussed in Sections 2 and 3, and explicit formulae are derived in Section 4 for the components of the pressure and pressure gradient attributable to the displacement of air by the moving train, and to the exit flows of the displaced air from the hood and from the tunnel into the hood. The formulae are applied in Section 5, where a comparison is made with model scale experiments conducted at train Mach numbers as large as 0.29 ($U\sim 350$ kph). The appendix contains further details of the derivation of the approximate Green's function discussed in Section 3.

The recent paper by Bellenoue et al. (2001) appeared after the present article had been submitted for publication. These authors report a series of model scale tests similar to those discussed below, using an unvented uniform hood with $M\leqslant 0.14$ ($U\leqslant 170$ kph) and for several different hood lengths. The results of these tests were used to devise an empirical scheme for the prediction of compression wave properties, but no attempt was made to develop and validate a rational theory of compression wave formation of the kind presented in this paper.

2. Equation governing compression wave formation

The Reynolds number of the air flow induced by a high-speed train entering a tunnel is large enough for the initial interactions of the train and tunnel to be regarded as inviscid. This means that the characteristics of compression wave formation will scale predominantly on the train Mach number M and on the blockage $\mathscr{A}_o/\mathscr{A}$, and that experiments conducted at model scale will provide a faithful representation of full scale results provided the Mach number and relative geometrical sizes of the tunnel and train are the same (Ozawa et al., 1976, 1988a). The model scale experiments described later in this paper are performed at roughly 1/127 of full-scale using the arrangement shown schematically in Fig. 1 (described in greater detail in Section 5). The main body of the tunnel consists of a uniform, rigid walled circular cylindrical duct of radius R (= 5 cm) and cross-sectional area $\mathscr{A}=\pi R^2$. The tunnel entrance is fitted with an unvented, coaxial cylindrical 'hood' of radius $R_h>R$, cross-sectional area $\mathscr{A}_h=\pi R_h^2$, and of length $\ell_h\gg R_h$. The junction of the tunnel and hood is equivalent to a discontinuous change in the tunnel radius.

Coordinates $\mathbf{x}=(x,y,z)$ are taken with the origin O on the axis of symmetry in the entrance plane of the hood, with the negative x-axis coinciding with the common axis of the tunnel and hood. In the experiments model, axisymmetric trains are projected from $x>0$ into the hood along its axis, and measurements are made of the compression wave radiated into the tunnel by means of pressure sensors in the tunnel walls about 1 m from the junction of the tunnel and hood. In a long tunnel the initial waveform is independent of the length of the tunnel, which may therefore be assumed to extend to $x=-\infty$ for the purposes of calculating the formation of the compression wave. The circular cross-section of the train becomes uniform with radius h and area $\mathscr{A}_o=\pi h^2$ at a distance L from the nose of the train. The train nose profile is assumed to be sufficiently streamlined that flow separation does not occur. During the formation of the compression wave the train speed is constant and equal to U in the negative x-direction. The Mach number $M=U/c_o$ does not normally exceed about 0.4, and the blockage $\mathscr{A}_o/\mathscr{A}$ is typically less than about 0.2.

The passage of the train produces variations in the air pressure $\bar{p}$, density ρ, and sound speed c, which are therefore functions of position $\mathbf{x}$ and time t; their corresponding undisturbed values are denoted by $p_o,\ \rho_o,\ c_o$. We shall neglect thermal and frictional losses during the formation of the compression wave, so that the air flow may be regarded as adiabatic and its unsteady motion can be calculated from the corresponding equation describing the generation of sound in the presence of a moving surface (Howe 1998a; Howe et al., 2000)

$$\left(\frac{\mathrm{D}}{\mathrm{D}t}\left(\frac{1}{c^2}\frac{\mathrm{D}}{\mathrm{D}t}\right)-\frac{1}{\rho}\nabla\cdot(\rho\nabla)\right)B=\frac{1}{\rho}\mathrm{div}(\rho\boldsymbol{\omega}\wedge\mathbf{v}),\tag{2.1}$$

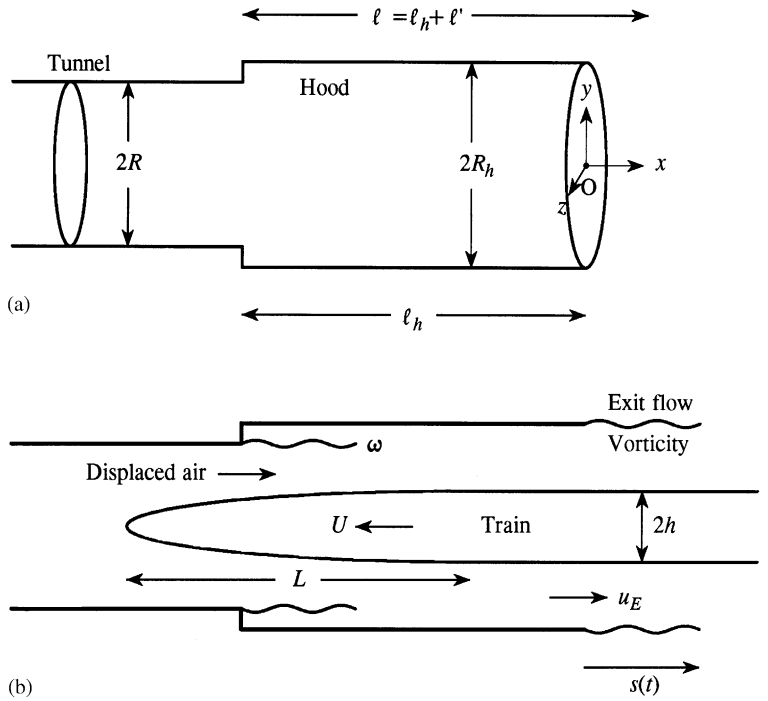

Fig. 1. (a) Schematic illustration of a circular cylindrical tunnel of radius R fitted with an unvented hood of radius R_h and length ℓ_h. The coordinate origin is at O at the centre of the hood entrance plane. (b) Parameters defining the axisymmetric train entering at speed U, showing the shear layers of the exit flows from the tunnel and hood.

where $\mathbf{v}(\mathbf{x}, t)$ is the velocity of the air, $\boldsymbol{\omega} = curl\,\mathbf{v}$ is the vorticity, and $B = \int \mathrm{d}\bar{p}/\rho(\bar{p}) + \frac{1}{2}v^2$ is the total enthalpy. The air may be regarded as linearly perturbed from its undisturbed state in the region ahead of the train, where

$$B \approx \frac{p}{\rho_o}, \quad p = \bar{p} - p_o. \tag{2.2}$$

In the absence of surface friction and of separation from the train, the vorticity $\boldsymbol{\omega}$ must vanish everywhere except within the shear layers of the exit flows from the entrance to the hood and from the tunnel into the hood produced by the air displaced by the advancing train (Fig. 1b). In the absence of the train B is constant throughout the fluid, and it may be assumed to vanish prior to the arrival of the train.

Two essentially distinct problems must be solved in order to use Eq. (2.1) to investigate the formation of the compression wave. First, it is necessary to specify a distribution of monopole and dipole sources that represent the presence of the moving train. These sources also determine the strength of the exit flow vortex source distribution shown explicitly on the right-hand side of Eq. (2.1). Second, the unsteady air motion produced by these sources must then be determined from Eq. (2.1) with proper account taken of boundary conditions on the inner and outer walls of the hood and tunnel. This interaction between the sources and the tunnel and hood governs the form of the compression wave profile. In this paper, and for the experiments discussed below, it is sufficient to consider the simplest case of *rigid* walls, on which the normal derivative $\partial B/\partial x_n = 0$.

The front of the moving train may be regarded as a set of monopole sources distributed over the nose region where the cross-sectional area of the train is variable; these monopoles account for the massive displacement of the air ahead of the advancing train. Their interaction with a hood, tunnel or other neighbouring structure produces a pressure excess over the nose of the train (i.e., a *drag* force) that is acoustically equivalent to a distribution of dipoles. In principle, the present method can be applied for any nose shape in the absence of separation. But Howe et al. (2000) showed how the monopole–dipole combination could be represented by the following slender body approximation:

$$U\left(1 + \frac{\mathscr{A}_o}{\mathscr{A}}\right)\frac{\partial}{\partial t}\left(\frac{\partial \mathscr{A}_T}{\partial x}(x + Ut)\delta(y)\delta(z)\right). \tag{2.3}$$

In this formula $\mathscr{A}_T(s)$ is the cross-sectional area of the train at distance s *from the tip of the nose*, which is taken to cross the entrance plane of the hood at time $t = 0$. The approximation replaces the exact monopole and dipole distributions,

which should strictly be distributed over the bounding surface of the train, by a line source along the axis of the train over the interval in which the nose area is variable. Thus, the source strength is proportional to the rate at which the cross-section changes with distance along the train, and is nonzero only in the vicinity of the train nose. The component of Eq. (2.3) involving the factor $\mathscr{A}_o/\mathscr{A}$ represents the contribution from the drag dipole, and the approximation is expected to be valid at least for $\mathscr{A}_o/\mathscr{A} \leqslant 0.2$, which covers all practical situations at full-scale involving operations at high speed. It will be assumed that the train is sufficiently long that it is permissible to ignore the influence of a similar distribution of sources near the tail, at least when attention is confined to the formation of the compression wave.

A further correction can be applied to the slender body approximation Eq. (2.3) that greatly simplifies the calculation of the compression wave at higher Mach numbers M. This was also discussed by Howe et al. (2000), who showed that compression wave predictions obtained in the limit $M \to 0$ could be extrapolated to finite values of M (less than about 0.4) by multiplying by $1/(1-M^2)$. In the same low Mach number approximation, departures of the density ρ from the mean air density ρ_o in the vortex source on the right of Eq. (2.1) can be ignored. Finally, if the small effects of nonlinearity on the *propagation* of the compression wave are also ignored, the left-hand side of the exact Eq. (2.1) can be linearized and the formation of the compression wave is found to be governed by

$$\left(\frac{1}{c_o^2}\frac{\partial^2}{\partial t^2} - \nabla^2\right) B = \frac{U}{(1-M^2)}\left(1 + \frac{\mathscr{A}_o}{\mathscr{A}}\right)\frac{\partial}{\partial t}\left(\frac{\partial \mathscr{A}_T}{\partial x}(x+Ut)\delta(y)\delta(z)\right) + \mathrm{div}(\boldsymbol{\omega} \wedge \mathbf{v}). \tag{2.4}$$

The neglect of nonlinear propagation terms on the left-hand side implies that the solution will determine only the *initial* shape of the compression wave profile, before the onset of wave steepening, i.e., that the solution is applicable only within the region several tunnel diameters ahead of the train, during and just after tunnel entry.

3. Green's function

The solution of Eq. (2.4) will be derived by the method discussed by Howe (1998b), in terms of a Green's function $G(\mathbf{x}, \mathbf{x}', t-\tau)$ that has vanishing normal derivative $\partial G/\partial x_n$ on the tunnel walls, and satisfies

$$\left(\frac{1}{c_o^2}\frac{\partial^2}{\partial t^2} - \nabla^2\right) G = \delta(\mathbf{x}-\mathbf{x}')\delta(t-\tau),$$
$$G = 0 \quad \text{for } t < \tau. \tag{3.1}$$

It is not possible to determine a closed form representation for G that is valid under all circumstances. However, an excellent analytical approximation is available that is applicable at all train speeds (say, $U \leqslant 500$ kph) for which the thickness of the compression wavefront is much larger than the tunnel diameter.

Introduce the labelling T, J, H, E, and A shown in the schematic Fig. 2 of different parts of the tunnel and hood, corresponding, respectively, to the uniform tunnel of radius R, the junction between the tunnel and hood, the mid-region of the hood of length $\ell_h \gg R_h$, the hood entrance, and the neighbouring free space outside the hood. The Green's function approximation involves a potential function $\varphi^*(\mathbf{x})$ that satisfies Laplace's equation and represents the velocity potential of a hypothetical incompressible, irrotational flow *out* of the mouth E of the hood from $x = -\infty$, and is normalized such that

$$\varphi^*(\mathbf{x}) \sim \begin{cases} x - \ell' & \text{when } |x| \gg R_h \text{ in the region } H \text{ within the hood,} \\ \dfrac{-\mathscr{A}_h}{4\pi|\mathbf{x}|} & \text{when } |\mathbf{x}| \gg R_h \text{ in the region } A \text{ outside the hood,} \end{cases} \tag{3.2}$$

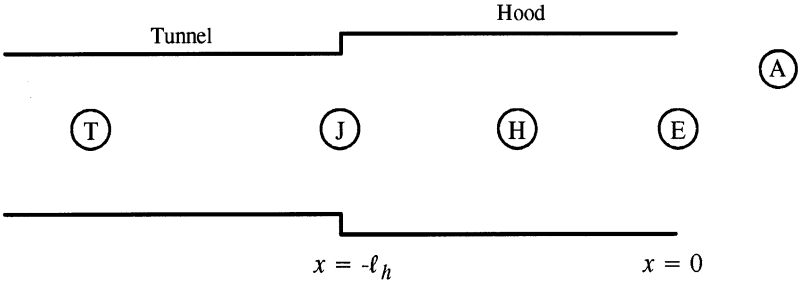

Fig. 2. Regions T, J, H, E, and A of the tunnel and hood used to define the Green's function. The coordinate origin is at the hood entrance plane.

where $\ell' \approx 0.61 R_h$ is the 'end-correction' of the hood mouth (Rayleigh, 1926). The function $\varphi^*(\mathbf{x})$ varies continuously through the hood mouth, in the neighbourhood of which $\varphi^*(\mathbf{x}) \sim O(R_h)$.

It is known from potential theory (Lamb, 1932; Noble, 1958; Milne-Thomson, 1968) that, when ℓ_h exceeds about $4R_h$ the potential $\varphi^*(\mathbf{x})$ can be approximated in regions H, E and A by the potential $\varphi^*_E(\mathbf{x})$, say, that describes uniform flow from the mouth of a *semi-infinite* hood of radius R_h (and which also satisfies the normalization conditions (3.2)). A convenient analytical representation of this function is given in Section A.1 of Appendix A. Similarly, in the neighbourhood of the junction J (near $x = -\ell_h$) we can set

$$\varphi^*(\mathbf{x}) = \frac{\mathscr{A}_h}{\mathscr{A}} \varphi^*_J(\mathbf{x}) - \ell, \quad \ell = \ell_h + \ell', \tag{3.3}$$

where to an excellent approximation $\varphi^*_J(\mathbf{x})$ coincides with the velocity potential of incompressible flow through the junction of two *semi-infinite* cylindrical ducts, satisfying

$$\varphi^*_J(\mathbf{x}) \sim \begin{cases} x + \ell_h - \ell_j & \text{when } |x + \ell_h| \gg R \text{ in the region } T \text{ of the tunnel,} \\ \dfrac{\mathscr{A}}{\mathscr{A}_h}(x + \ell_h) & \text{when } |x + \ell_h| \gg R_h \text{ in the region } H \text{ of the hood,} \end{cases} \tag{3.4}$$

where $\ell_j \ll R$ is the effective 'length' of the junction defined by Eq. (A.1) of Appendix A. The behaviour of $\varphi^*_J(\mathbf{x})$ in the vicinity of the junction can therefore be obtained in a routine manner using, say, a finite difference approximation to the equations for potential flow through a discontinuous change in cross-section in a circular duct infinite in both directions.

The compression wave is generated by the interaction of the train nose with ends E and J of the hood. These interactions are essentially independent when $\ell_h \gg R_h$, and localized to the immediate neighbourhoods of E and J. It will be shown below that this localization occurs because $\partial^2\varphi^*/\partial x^2$ vanishes everywhere except in the neighbourhoods of E and J, and that it is therefore permissible to write

$$\frac{\partial^2 \varphi^*}{\partial x^2} = \frac{\partial^2 \varphi^*_E}{\partial x^2} + \frac{\mathscr{A}_h}{\mathscr{A}} \frac{\partial^2 \varphi^*_J}{\partial x^2}.$$

Fig. 3 shows a plot of the variation of $\partial^2\varphi^*/\partial x^2$ on the axis of symmetry of the tunnel and hood for $\ell_h = 10R$, $R_h = 1.25R$ (the case examined experimentally in this paper).

In terms of these definitions: in the particular case in which the observation point $\mathbf{x}$ lies in the acoustic far field of the hood within the tunnel T, and the source point $\mathbf{x}'$ is in H or in the vicinity of the ends E and J of the hood, it is shown in Section A.2 that the approximate form of $G(\mathbf{x}, \mathbf{x}'; t - \tau)$ is given by

$$G(\mathbf{x}, \mathbf{x}'; t - \tau) = \frac{c_o \mathscr{T}_J}{2\mathscr{A}_h} \sum_{n=0}^{\infty} \mathscr{R}_E^n \mathscr{R}_J^n \left\{ \mathrm{H}\left([t] - \tau - \frac{(2n\ell + \varphi^*(\mathbf{x}))}{c_o} \right) + \mathscr{R}_E \mathrm{H}\left([t] - \tau - \frac{(2n\ell - \varphi^*(\mathbf{x}'))}{c_o} \right) \right\},$$
$$x \to -\infty, \tag{3.5}$$

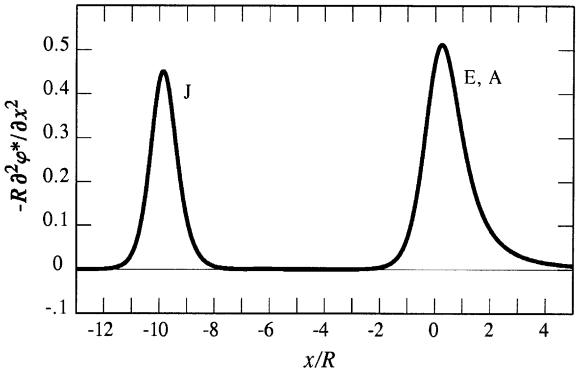

Fig. 3. Variation of $-R\partial^2\varphi^*/\partial x^2$ on the axis of symmetry of the tunnel and hood for $\ell_h = 10R$, $R_h = 1.25R$: where

$$\frac{\partial^2 \varphi^*}{\partial x^2} = \frac{\mathscr{A}_h}{\mathscr{A}} \frac{\partial^2 \varphi^*_J}{\partial x^2} \text{ at } J \quad \text{and} \quad = \frac{\partial^2 \varphi^*_E}{\partial x^2} \text{ at } E \text{ and } A.$$

where H is the Heaviside step function, $[t] = t + (x - \ell')/c_o$ is the retarded time, and

$$\mathscr{R}_E = -1, \quad \mathscr{R}_J = \frac{\mathscr{A}_h - \mathscr{A}}{\mathscr{A}_h + \mathscr{A}}, \quad \mathscr{T}_J = \frac{2\mathscr{A}_h}{\mathscr{A}_h + \mathscr{A}}. \tag{3.6}$$

The constants $\mathscr{R}_E$, $\mathscr{R}_J$, $\mathscr{T}_J$ have the following significance (see Lighthill's (1978) discussion of sound transmission and reflection at compact area changes and junctions in channels): for sound of wavelength λ, $\mathscr{R}_E$ is the limiting value for $\lambda \gg R$ of the acoustic plane wave reflection coefficient at the open end of the hood; $\mathscr{R}_J$ is the corresponding limit for reflection at the junction end of the hood *back into* the hood; and $\mathscr{T}_J$ is the limiting value of the transmission coefficient for a plane wave transmitted from the hood into the tunnel. Representation (3.5) is uniformly valid for source positions $\mathbf{x}'$ lying within the hood or the neighbourhood of its open end and the junction with the tunnel.

To understand the terms in the brace brackets of Eq. (3.5), consider the case where the source point $\mathbf{x}'$ lies in the body of the hood. For $n = 0$ the first Heaviside function represents the front of the disturbance radiated into the tunnel; the second is the contribution from the wavefront that initially propagates towards the hood entrance, where it is reflected with reflection coefficient $\mathscr{R}_E = -1$ and subsequently radiated into the tunnel; the amplitude of each of these 'direct' waves is *increased* on transmission into the tunnel across the contraction in cross-sectional area at the junction because the transmission coefficient $\mathscr{T}_J > 1$ (see Lighthill, 1978). The terms in $n \geqslant 1$ represent contributions arriving at later times, after the transmission into the tunnel of those components of the direct waves that have suffered n reflections from both ends of the hood; the amplitude decreases by a factor $\mathscr{R}_J < 1$ on each reflection back into the hood from the junction with the tunnel, so that the higher order modes rapidly decrease in amplitude.

4. Calculation of the compression wave

In the linearly disturbed air in the tunnel ahead of the train $B \approx p/\rho_o$, and according to Eq. (2.4) two distinct sources contribute to the pressure p. We shall write

$$p = p_T + p_\omega, \tag{4.1}$$

where the pressure components on the right-hand side correspond, respectively, to the contributions from the first and second source terms in Eq. (2.4), from the moving train and from the shear layers in the exit flows from the tunnel and hood. It can be anticipated that $p_T \gg p_\omega$.

4.1. Evaluation of p_T

At points $\mathbf{x}$ within the tunnel, ahead of the train, we have

$$p_T \equiv p_T([t]) = \frac{\rho_o U}{(1 - M^2)}\left(1 + \frac{\mathscr{A}_o}{\mathscr{A}}\right)\frac{\partial}{\partial t}\int\int_{-\infty}^{\infty} \frac{\partial \mathscr{A}_T}{\partial x'}(x' + U\tau)G(\mathbf{x}, x', 0, 0; t - \tau)\,\mathrm{d}x'\,\mathrm{d}\tau, \tag{4.2}$$

where G is given by Eq. (3.5). The integrand is nonzero only in the neighbourhoods of the nose and tail of the train, where the cross-sectional area $\mathscr{A}_T$ is changing. The compression wave is generated in two stages, as the nose enters the hood, and as it crosses the junction with the tunnel, and its explicit form is calculated by temporarily considering a train of semi-infinite length.

For noise control purposes the pressure 'gradient' $\partial p/\partial t$ is the principal quantity of interest. By invoking the identity

$$\frac{\partial \mathscr{A}_T}{\partial t}(x + Ut) = U\frac{\partial \mathscr{A}_T}{\partial x}(x + Ut) \tag{4.3}$$

and integrating by parts, we find

$$\frac{\partial p_T}{\partial t} = \frac{\rho_o U^3}{(1 - M^2)}\left(1 + \frac{\mathscr{A}_o}{\mathscr{A}}\right)\int\int_{-\infty}^{\infty} \frac{\partial \mathscr{A}_T}{\partial x'}(x' + U\tau)\frac{\partial^2 G}{\partial x'^2}(\mathbf{x}, x', 0, 0; t - \tau)\,\mathrm{d}x'\,\mathrm{d}\tau. \tag{4.4}$$

The second-order derivative $\partial^2 G/\partial x'^2$ is evaluated from Eq. (3.5) by observing that at small Mach numbers (when the compression wavefront thickness $\gg R$, R_h)

$$\frac{\partial^2 \mathrm{H}}{\partial x'^2}\left([t] - \tau - \frac{(2n\ell \pm \varphi^*(\mathbf{x}'))}{c_o}\right) \approx \mp\frac{1}{c_o}\frac{\partial^2 \varphi^*}{\partial x'^2}(\mathbf{x}')\,\delta\left([t] - \tau - \frac{(2n\ell \pm \varphi^*(\mathbf{x}'))}{c_o}\right), \tag{4.5}$$

the term omitted on the right-hand side being O(M) smaller. But $\partial^2\varphi^*/\partial x'^2$ is nonzero only in the immediate vicinities of the ends J and E of the hood, where, respectively,

$$\frac{\partial^2\varphi^*}{\partial x'^2} = \frac{\mathscr{A}_h}{\mathscr{A}}\frac{\partial^2\varphi^*_J}{\partial x'^2}, \quad \varphi^* \approx -\ell, \quad \text{and}$$
$$\frac{\partial^2\varphi^*}{\partial x'^2} = \frac{\partial^2\varphi^*_E}{\partial x'^2}, \quad \varphi^* \approx 0. \tag{4.6}$$

Hence, Eq. (4.4) becomes

$$\frac{\partial p_T}{\partial t} = \frac{-\rho_o U^3}{\mathscr{A}_h(1-M^2)}\left(1+\frac{\mathscr{A}_o}{\mathscr{A}}\right)\mathscr{T}_J\sum_{n=0}^{\infty}(-1)^n\mathscr{R}_J^n\int_{-\infty}^{\infty}\frac{\partial\mathscr{A}_T}{\partial x'}(x'+U[t]-2nM\ell)\frac{\partial^2\varphi^*_E}{\partial x'^2}(x',0,0)\,\mathrm{d}x'$$
$$-\frac{\rho_o U^3}{2\mathscr{A}(1-M^2)}\left(1+\frac{\mathscr{A}_o}{\mathscr{A}}\right)\mathscr{T}_J\sum_{n=0}^{\infty}(-1)^n\mathscr{R}_J^n\int_{-\infty}^{\infty}\left\{\frac{\partial\mathscr{A}_T}{\partial x'}(x'+U[t]-(2n-1)M\ell)\right.$$
$$\left.+\frac{\partial\mathscr{A}_T}{\partial x'}(x'+U[t]-(2n+1)M\ell)\right\}\frac{\partial^2\varphi^*_J}{\partial x'^2}(x',0,0)\,\mathrm{d}x'. \tag{4.7}$$

The first line in this equation represents all components of the pressure gradient produced by the interaction of the train with the entrance to the hood; the second term on the right consists of all those waves generated at time $\sim\ell_h/U$ later, as the train passes into the tunnel from the hood.

Because the derivatives $\partial^2\varphi^*_{E,J}/\partial x^2$ are strongly localized and sharply peaked functions (Fig. 3), solution (4.7) describes a pressure gradient $\partial p_T/\partial t$ consisting of a succession of pulses, the later ones being transmitted from the hood into the tunnel after being temporarily confined to the hood by reflection from its ends. The amplitudes of the waves trapped within the hood progressively decrease (by a factor $\mathscr{R}_J$ at each reflection from the junction of the tunnel and hood) as wave energy escapes into the tunnel, so that the amplitudes of the later pulses also decrease. The decrease is fairly rapid in practice, and the first two or three terms in each of the infinite series in Eq. (4.7) are generally sufficient to describe the growth of the compression wave. In reality, of course, the solution ceases to be applicable at larger retarded times when the later pulses are emitted, because of interference caused by the arrival of the tail of the train, and because of frictional and turbulence losses (the latter is discussed further in Section 6).

The integrations in Eq. (4.7) must normally be performed numerically, after which the corresponding pressure p_T is most easily determined by evaluating

$$p_T(t) = \int_{-\infty}^{t}\frac{\partial p_T}{\partial t'}(t')\,\mathrm{d}t'. \tag{4.8}$$

The limiting value of this integral as $t\to+\infty$ is just the total pressure rise Δp_T, say, across the compression wave. It can be verified from Eq. (4.7) that this pressure rise is precisely that quoted above in Eq. (1.1). To do this the integrals in Eq. (4.7) are first transformed into exact differentials with respect to time by integrating by parts with respect to x' (thereby transferring an additional partial derivative $\partial/\partial x'$ onto $\partial\mathscr{A}_T/\partial x'$) and using identity (4.3). Then, because the derivatives $\partial\varphi^*_{E,J}/\partial x'$ assume constant values at $x'=\pm\infty$, and $\int_{-\infty}^{\infty}(\partial\mathscr{A}_T/\partial x')\,\mathrm{d}x' = \mathscr{A}_o$ (when the tail of the train is ignored), we find

$$\Delta p_T = \frac{\rho_o U^2}{(1-M^2)}\left(1+\frac{\mathscr{A}_o}{\mathscr{A}}\right)\mathscr{T}_J\sum_{n=0}^{\infty}(-1)^n\mathscr{R}_J^n\left\{\frac{\mathscr{A}_o}{\mathscr{A}_h}\left[\frac{\partial\varphi^*_E}{\partial x'}\right]_{\infty}^{-\infty}+\frac{\mathscr{A}_o}{\mathscr{A}}\left[\frac{\partial\varphi^*_J}{\partial x'}\right]_{\infty}^{-\infty}\right\}.$$

The equivalence of this result and the pressure rise of Eq. (1.1) now follows from the asymptotic relations (3.2), (3.4), and by noting that $\mathscr{T}_J\sum_{n=0}^{\infty}(-1)^n\mathscr{R}_J^n = 1$.

4.2. The vortex pressure p_ω

Boundary layer vorticity (i.e., the effect of 'skin friction') on the train and tunnel walls becomes progressively more important as a source of tunnel pressure fluctuations after the entry of the train nose into the tunnel, and after the formation of the major part of the compression wave. At large times the boundary layers on the tunnel and train diffuse and merge and lead to an effective increase in the monopole strength of the nose that strongly influences the later stages of the development of the wave. Vortex energy is also transformed into low-frequency pressure transients propagating within the tunnel because of hydrodynamic interactions with structural irregularities (Howe, 1998a). In our case the hood entrance and the junction between the tunnel and hood are the most important irregularities. Also important is

the free shear layer vorticity formed at the outer edge of the annular jet ejected from the hood when the nose crosses the entrance plane, and from the tunnel entrance when the train nose crosses the junction between the hood and tunnel (Auvity and Bellenoue, 1998; Auvity et al., 2001). The vortex source is naturally of secondary importance relative to the monopole and dipole sources responsible for the component p_T. However, it was shown by Howe et al. (2000) to give a small but finite contribution immediately on entry of a train into a tunnel with no hood, and to produce a measurable effect on the initial waveform,

We shall therefore ignore the boundary layer contributions from the train and tunnel walls (important at later times, see Section 6), and estimate only the additional pressure produced by the 'exit flow' vorticity using for this purpose the second source term on the right of Eq. (2.4). According to Fig. 1b there are two exit flow regions: from the hood at E, and from the tunnel to the hood at J. Let the respective contributions to the pressure be denoted by

$$p_\omega = p_\omega^E + p_\omega^J. \tag{4.9}$$

The procedure for calculating these pressures is very similar to that discussed by Howe et al. (2000) in the absence of a hood.

The exit flow shear layers will in practice roll-up to form discrete vortices, but immediately after the train nose enters the hood, say, the initial vorticity may be regarded as confined to a circular cylindrical vortex sheet marking the outer boundary of a uniform jet of radius R_h exhausting from the hood at speed $u_E(t)$ in the x-direction. Then

$$\mathrm{div}(\boldsymbol{\omega}\wedge\mathbf{v}) = \begin{cases} \frac{R_h}{r}\frac{\partial}{\partial r}(\tfrac{1}{2}u_E^2\delta(r-R_h)), & 0<x<s(t), \\ 0 & \text{elsewhere}, \end{cases} \tag{4.10}$$

where $s(t)$ is the length of the jet outside the hood, as indicated in Fig. 1b, and $r=\sqrt{y^2+z^2}$ is radial distance from the x-axis.

The velocity $u_E(t)$ increases from zero to a constant value $\sim U\mathscr{A}_o/\mathscr{A}_h$ during the time $\sim L/U$ required for the train nose to enter the hood. The flow occurs at sufficiently low Mach number to be regarded as incompressible, so that we can take $u_E(t)=U\mathscr{A}_T(Ut)/\mathscr{A}_h$ for $0<t<L/U$. The length $s(t)$ of the jet and shear layer is given by $s(t)=\int_0^t u_E(\tau)\,\mathrm{d}\tau$, $t>0$. Hence, by first noting from Eq. (3.5) that the $\mathbf{x}'$-dependent part of $G(\mathbf{x},\mathbf{x}',t-\tau)$ near E has the form

$$G(\mathbf{x},\mathbf{x}',t-\tau)\approx\frac{-\varphi_E^*(\mathbf{x}')\mathscr{T}_J}{\mathscr{A}_h}\sum_{n=0}^{\infty}(-1)^n\mathscr{R}_J^n\delta\left([t]-\tau-\frac{2n\ell}{c_o}\right),\quad x\to-\infty, \tag{4.11}$$

it is found that the pressure p_ω^E attributable to the shear layers outside the hood can be cast in the form

$$p_\omega^E([t])\approx\frac{\rho_o U^2}{2\mathscr{A}_h}\mathscr{T}_J\sum_{n=0}^{\infty}(-1)^n\mathscr{R}_J^n\mathrm{H}(\tau_{2n})\left(\frac{\mathscr{A}_T(U\tau_{2n})}{\mathscr{A}_h}\right)^2\int_0^{s(\tau_{2n})}2\pi R_h\left(\frac{\partial\varphi_E^*}{\partial r'}\right)_{r'=R_h}\mathrm{d}x',$$

where

$$\tau_N=[t]-\frac{N\ell}{c_o},\quad r'=\sqrt{y'^2+z'^2}. \tag{4.12}$$

The integral can be interpreted as the volume flux through the boundary of the jet (of length s) of a hypothetical incompressible flow from the hood defined by the velocity potential φ_E^*, and can be evaluated explicitly in terms of the corresponding Stokes stream function $\psi_E^*(r',x')$ (Lamb, 1932), which satisfies

$$\frac{1}{r'}\frac{\partial\psi_E^*}{\partial r'}=\frac{\partial\varphi_E^*}{\partial x'},\quad \frac{1}{r'}\frac{\partial\psi_E^*}{\partial x'}=-\frac{\partial\varphi_E^*}{\partial r'}.$$

$\psi_E^*(R_h,x')=\mathscr{A}_h/2\pi$ at the exit $x'=0$ of the hood, and decreases smoothly to zero as $x'\to+\infty$, and therefore

$$p_\omega^E([t])\approx\frac{\rho_o U^2}{2}\mathscr{T}_J\sum_{n=0}^{\infty}(-1)^n\mathscr{R}_J^n\mathrm{H}(\tau_{2n})\left(\frac{\mathscr{A}_T(U\tau_{2n})}{\mathscr{A}_h}\right)^2\left(1-\frac{2\pi\psi_E^*(R_h,s(\tau_{2n}))}{\mathscr{A}_h}\right). \tag{4.13}$$

The term in $n=0$ in this formula gives the direct wave generated by the jet which passes into the tunnel with its amplitude increased by the factor $\mathscr{T}_J$; the component for each $n>0$ has been reflected n times at the junction and at the open end of the hood before escaping into the tunnel.

A similar calculation can be performed to determine the component p_ω^J of the compression wave generated by the free shear layers in the jet flow from the tunnel at J. In this case we can take, near J,

$$G(\mathbf{x},\mathbf{x}',t-\tau)\approx\frac{-\varphi_J^*(\mathbf{x}')\mathscr{T}_J}{2\mathscr{A}}\sum_{n=0}^{\infty}(-1)^n\mathscr{R}_J^n\left\{\delta\left([t]-\tau-\frac{(2n-1)\ell}{c_o}\right)+\delta\left([t]-\tau-\frac{(2n+1)\ell}{c_o}\right)\right\},\quad x\to-\infty, \tag{4.14}$$

to find

$$p'^{J}_{\omega}([t]) \approx \frac{\rho_o U^2}{4}\mathscr{T}_J \sum_{n=0}^{\infty}(-1)^n \mathscr{R}_J^n \left\{ \mathrm{H}(\tau'_{2n-1})\left(\frac{\mathscr{A}_T(U\tau'_{2n-1})}{\mathscr{A}}\right)^2\left(1-\frac{2\pi\psi^*_J(R,s(\tau_{2n-1})-\ell_h)}{\mathscr{A}}\right)\right.$$
$$\left. + \mathrm{H}(\tau'_{2n+1})\left(\frac{\mathscr{A}_T(U\tau'_{2n+1})}{\mathscr{A}}\right)^2\left(1-\frac{2\pi\psi^*_J(R,s(\tau_{2n+1})-\ell_h)}{\mathscr{A}}\right)\right\},$$
$$x\to-\infty, \tag{4.15}$$

where

$$\tau'_N = \tau_N - \frac{\ell_h}{U} \equiv [t] - \frac{N\ell}{c_o} - \frac{\ell_h}{U},$$

and $\psi^*_J(\mathbf{x}') \equiv \psi^*_J(r', x')$ is the stream function corresponding to φ^*_J, defined such that

$$\psi^*_J(R,-\ell_h) = \frac{\mathscr{A}}{2\pi}, \quad \psi^*_J(R,+\infty) = \frac{\mathscr{A}^2}{2\pi\mathscr{A}_h}. \tag{4.16}$$

The additional time delay equal to ℓ_h/U in τ'_N arises because the exit flow from the tunnel does not begin until the train nose arrives at the junction between the hood and tunnel after traversing the length ℓ_h of the hood.

Note that the same numerical computation required to determine φ^*_J also yields the Stokes stream function ψ^*_J; similarly, the analytical formula given in the appendix for φ^*_E determines also ψ^*_E.

5. Comparison with experiment

5.1. Experimental apparatus and the instrumentation

The model scale experiments were performed at the Railway Technical Research Institute in Tokyo using the apparatus illustrated schematically in Fig. 4. The uniform section of the tunnel consists of a 7 m long horizontal, unflanged, circular cylindrical pipe made of hard vinyl chloride, with inner and outer diameters respectively equal to 10 and 11.4 cm. Axisymmetric model trains are projected at high speed into the tunnel, guided by a 5 mm diameter taut steel wire extending along the tunnel axis. The tunnel entrance is fitted with an unvented entrance hood.

The train is launched by a three-stage friction drive involving three pairs of vertically aligned wheels (a greatly improved version of the apparatus described by Howe et al., 2000). It is accelerated up to a maximum speed of about 450 kph, the actual speed being controlled by varying the rates of rotation of the drive wheels. A 3.75 m long 'open' section between the launcher and the hood entrance is large enough to ensure that the spherically spreading pressure waves generated during the rapid acceleration of the train are negligible at the hood entrance. On emerging from the far end of the tunnel the train is brought to rest by a 'catcher' that slides along the steel wire, the motion being damped by a cloth and sponge shock-absorber. The catcher contains an air damper and fabric material to absorb the kinetic energy of the rapidly decelerating train, which is recovered without damage and can be used repeatedly in further tests.

Pressure measurements are made within the tunnel using two wall-mounted transducers, respectively, at 1.5 and 2.5 m from the hood entrance. The pressures are recorded continuously until the rarefaction wave produced by the reflection of the compression wave at the far tunnel exit is first detected by the second transducer. For all of the

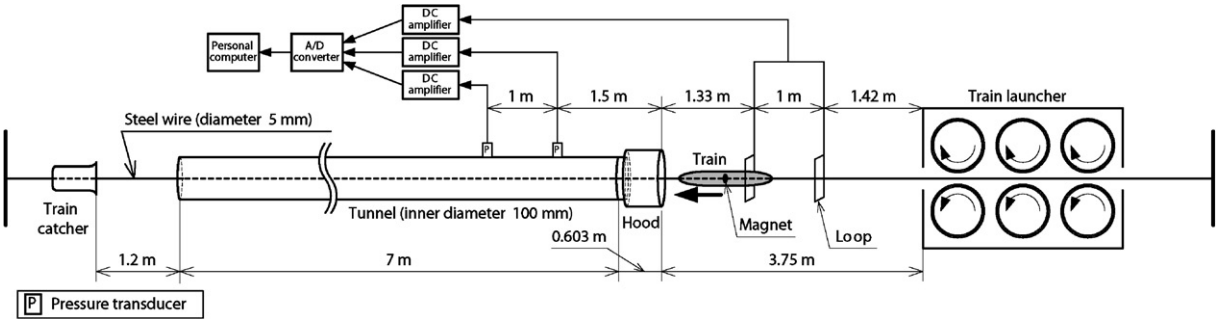

Fig. 4. Schematic of the experimental apparatus.

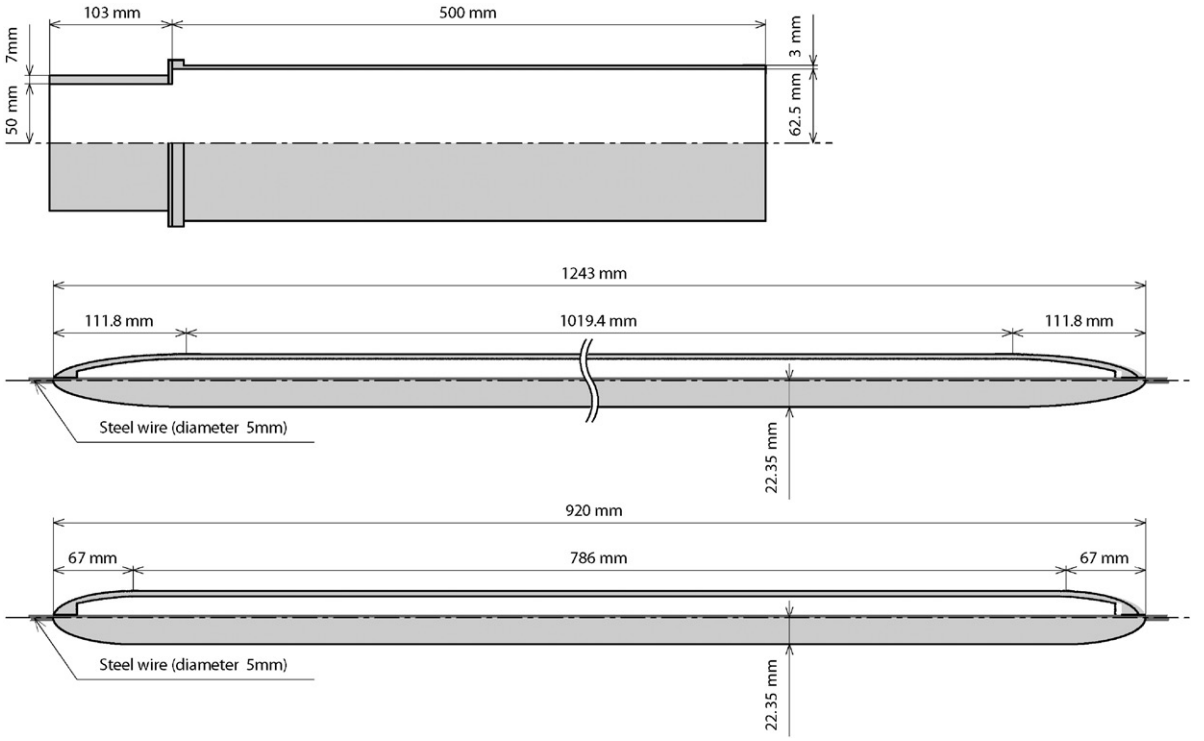

Fig. 5. (a) The unvented entrance hood fitted to the end of the circular cylindrical tunnel. (b) The long nose model train (i) with ellipsoidal nose and tail. (c) The short nose model train (ii) with ellipsoidal nose and tail.

measurements described here this occurs at least 15 ms after the arrival at the second transducer of the rarefaction wave generated when the tail of the train enters the hood.

The dimensions of the hood are shown in Fig. 5a. The hood consists of a circular cylindrical, vinyl chloride pipe of inner and outer diameters equal to 12.5 and 13.1 cm, respectively; a 10 cm collar at one end facilitates an airtight and smooth mating with the circular cylindrical tunnel. When in place the hood has an overall length of 60.3 cm, and a 'working length' of $\ell_h = 50$ cm. Thus, in the notation of Sections 2–4,

$$R = 5 \text{ cm}, \quad R_h = 1.25R, \quad \ell_h = 10R, \tag{5.1}$$

and $\mathscr{A}_h/\mathscr{A} = 1.5625$.

Two axisymmetric model trains (i) and (ii) were used in the experiments (see Figs. 5b and c), each with an ellipsoidal nose profile obtained by rotating the curve $y = h\sqrt{(x/L)(2 - x/L)}$, $0 < x < L$ about the x-axis, so that

$$\frac{\mathscr{A}_T(x)}{\mathscr{A}_o} = \begin{cases} \frac{x}{L}(2 - \frac{x}{L}), & 0 < x < L, \\ 1, & x > L, \end{cases} \tag{5.2}$$

where $\mathscr{A}_o = \pi h^2$. The trains had fore-aft symmetry, with equal nose and tail profiles, and the dimensions given in Table 1:

The trains are constructed using a nylon plastic material of total mass 920 g for model (i) and 640 g for (ii). The steel guide-wire passes axisymmetrically through a cylindrical hole in the train of diameter 5.5 mm. For these dimensions the blockage $\mathscr{A}_o/\mathscr{A} = 0.2$ (or 0.198 if account is taken of the cross-sectional area of the guide-wire), which is typical of the larger values arising in practice, where for high-speed operations ($U > 200$ kph) $\mathscr{A}_o/\mathscr{A}$ is usually restricted to the range 0.12–0.22.

The pressure measurements were made using two wall mounted *Toyoda Machine Works PD104K* transducers. The data were passed through a *Toyoda Machine Works AA6210* amplifier, digitized using a 12-bit analogue-to-digital converter with a sampling rate of 25 kHz per channel, and stored in a personal computer. The pressure gradient ($\mathrm{d}p/\mathrm{d}t$) was calculated using a central difference scheme after high-frequency components (> 1 kHz) of the measured pressure were removed using a fast fourier transform (FFT) algorithm. (The FFT coefficients of frequency higher than 1 kHz

Table 1
Dimensions of experimental trains

Model	Uniform radius h (cm)	Nose/tail length L (cm)	Overall length (cm)
(i)	2.235	11.18	124.3
(ii)	2.235	6.70	92.0

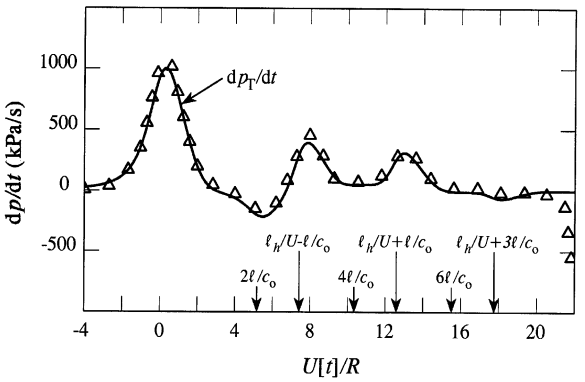

Fig. 6. The compression wave pressure gradient for train model (i) with the ellipsoidal nose profile defined by Eq. (5.2) entering at $U = 294$ kph a circular cylindrical tunnel with an unvented hood when $R = 5$ cm, $R_h = 1.25R$, $\ell_h = 10R$. The open triangles ($\triangle\ \triangle\ \triangle$) are the measured pressure gradient at a distance of 1.5 m from the hood entrance plane. The solid curve is prediction (5.3) of the component $\partial p_T/\partial t$ of the pressure gradient attributable to the moving train alone.

were set equal to zero and the smoothed pressure gradient was then calculated from the inverse transform determined by the remaining nonzero coefficients.)

Small permanent magnets made of neodymium inserted in train model (ii) and two wire loops placed 1 m apart in the open section between the launcher and the hood entrance were used to measure the speed of model (ii), by detection of the magnetic field of the passing train. The speeds of both trains were also measured by the procedure described in detail by Howe et al. (2000), based on observations of the *hydrodynamic* field of the passing train within the tunnel. The two methods yield results that differ by less than 1%. Only the second method was used for model train (i). In either case the overall error of the speed measurement is estimated to be no more than about 1%. It was also estimated that the tolerance error in the train cross-section is about 1%. Hence, because the compression wave amplitude is proportional to $U^2\mathscr{A}_o/\mathscr{A}$ it can be concluded that the overall errors in measurements of the pressure and pressure gradient are respectively of order 3% and 4%.

5.2. The pressure gradient

In this section and in Section 5.3 a detailed comparison of theory and experiment is made for model (i).

The solid curve in Fig. 6 is the component $\partial p_T/\partial t$ of the pressure gradient attributable to the train (i) and predicted by Eq. (4.7) for $U = 294$ kph ($M = 0.24$). It is plotted as a function of the nondimensional retarded time $U[t]/R$, $[t] = t + (x - \ell')/c_o$, where the nose of the train crosses the entrance plane of the hood at $t = 0$. The open triangles are observed values of the pressure gradient measured in the tunnel at a distance of 1.5 m from the entrance plane of the hood. Terms of order n in the expansions in Eq. (4.7) represent contributions from waves that have been reflected n times from both ends of the hood before being transmitted into the tunnel, and their relative magnitudes decrease as the index n increases. When attention is confined to the formation of the compression wave the contributions from large values of n can be discarded. Indeed, the tail of the experimental train enters the hood at $U[t]/R \sim 22$ (causing the pressure gradient to become negative, as indicated in the figure), so that Eq. (4.7) and the cross-sectional area

distribution (5.2) cease to represent the measured pressure gradient for larger times. The contributions from those wave components n of Eq. (4.7) that appear at larger times may therefore be discarded. In fact,

$$\mathscr{R}_J = 0.22, \quad \mathscr{T}_J = 1.22,$$

so that the higher order terms decrease rapidly in amplitude. In calculating the solid curve in Fig. 6 Eq. (4.7) has been approximated by

$$\frac{\partial p_T}{\partial t} = \frac{-\rho_o U^3}{\mathscr{A}(1-M^2)}\left(1+\frac{\mathscr{A}_o}{\mathscr{A}}\right)\mathscr{T}_J\left\{\frac{\mathscr{A}}{\mathscr{A}_h}\int_{-\infty}^{\infty}[\mathscr{A}'_T(x'+U[t]) - \mathscr{R}_J\mathscr{A}'_T(x'+U[t]-2M\ell) + \mathscr{R}_J^2\mathscr{A}'_T(x'+U[t]-4M\ell) - \mathscr{R}_J^3\mathscr{A}'_T(x'+U[t]-6M\ell)]\frac{\partial^2\varphi_E^*}{\partial x'^2}(x',0,0)\,\mathrm{d}x' + \frac{1}{2}\int_{-\infty}^{\infty}[\mathscr{A}'_T(x'+U[t]+M\ell) + (1-\mathscr{R}_J)\mathscr{A}'_T(x'+U[t]-M\ell) - \mathscr{R}_J(1-\mathscr{R}_J)\mathscr{A}'_T(x'+U[t]-3M\ell)]\frac{\partial^2\varphi_J^*}{\partial x'^2}(x',0,0)\,\mathrm{d}x'\right\}, \tag{5.3}$$

where the notation $\mathscr{A}'_T$ denotes differentiation with respect to x'.

To interpret this formula consider first the component

$$\mathscr{A}'_T(x'+U[t])\frac{\partial^2\varphi_E^*}{\partial x'^2}(x',0,0)$$

of the first integral: $\partial^2\varphi_E^*/\partial x'^2$ vanishes except close to $x'=0$ at the entrance to the hood; $\mathscr{A}'_T(x'+U[t])$ is nonzero only in the neighbourhood of the retarded position of the nose where $x'+U[t]=0$. Hence the first term in the first integral yields the leading pulse in Fig. 6, centered on $U[t]/R=0$. The three remaining terms in the first integral alternate in sign, and the same argument implies that they represent further contributions from the initial pulse reflected, respectively, once, twice and three times from the ends of the hood, and received at the corresponding retarded times

$$[t] = \frac{2\ell}{c_o}, \quad \frac{4\ell}{c_o}, \quad \frac{6\ell}{c_o}$$

indicated in the figure. The negative minimum of $\partial p_T/\partial t$ at $[t]=2\ell/c_o$ is caused by the first of these reflected pulses.

Similarly, in the second integral of Eq. (5.3) $\partial^2\varphi_J^*/\partial x'^2$ vanishes except near $x'=-\ell_h$ at the junction between the tunnel and hood. When the front of the train crosses the junction, at time $t=\ell_h/U$, a positive 'junction' pulse is radiated into the tunnel and an equal negative pulse is radiated back to the hood entrance. The first term in the second integral of Eq. (5.3) represents the forward radiated junction pulse, and is responsible for the second peak occurring near $[t]=\ell_h/U-\ell/c_o$ in Fig. 6. The second term in the second integral can be split as follows:

$$\mathscr{A}'_T(x'+U[t]-M\ell)\frac{\partial^2\varphi_J^*}{\partial x'^2}(x',0,0) - \mathscr{R}_J\mathscr{A}'_T(x'+U[t]-M\ell)\frac{\partial^2\varphi_J^*}{\partial x'^2}(x',0,0).$$

Here the first component is the contribution from the negative junction pulse after reflection from the hood entrance, whereas the second term is a second contribution from the positive junction pulse, part of which is reflected at the junction and again at the open end of the hood. Together these waves produce the third peak in Fig. 6 near $[t]=\ell_h/U+\ell/c_o$ with an amplitude that is smaller than the second peak radiated from the junction by a factor approximately equal to $1-\mathscr{R}_J\approx 0.78$. The final term in the second integral of Eq. (5.3) includes contributions from waves reflected once and twice at the ends of the hood but received at the same time $[t]\sim\ell_h/U+3\ell/c_o$; they produce the small but perceptible dip in the wave profile evident in both the experimental and theoretical results shown in the figure near this time.

5.3. The compression wave profile

The corresponding measured and predicted compression wave profiles for model (i) when $U=294$ kph are depicted in Fig. 7. As before the measurements are made in the tunnel 1.5 m from the entrance plane of the hood. The solid curve in the figure is the pressure p_T calculated from Eq. (4.8) using approximation (5.3) for $\partial p_T/\partial t$ displayed in Fig. 6. The agreement in Fig. 6 between the calculated $\partial p_T/\partial t$ and the measured pressure gradient is good, and the theory supplies a rational explanation for all of the observed maxima and minima. However, small differences in the absolute values of the measured $\partial p/\partial t$ and the calculated $\partial p_T/\partial t$ are sufficient to produce the noticeable differences evident in Fig. 7 at larger times in the measured pressure p and the component p_T attributable to the train alone.

Much of this difference is believed to be a consequence of flow separation on the train and tunnel or hood walls, and to the vorticity in the exit flow jets exhausting from the hood and tunnel, as discussed in Section 4.2. We shall use formulae (4.9), (4.13) and (4.15) to estimate the contribution from the exit flow jets. A more detailed comparison,

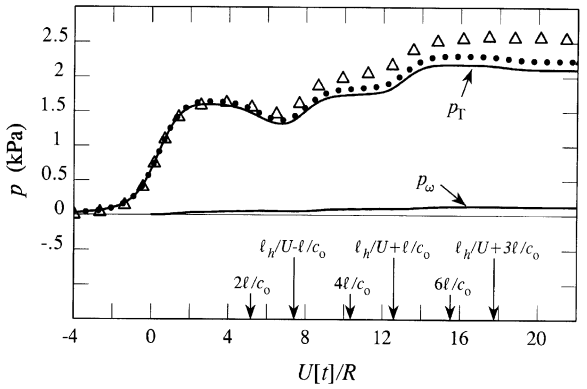

Fig. 7. The compression wave pressure for train model (i) with the ellipsoidal nose profile defined by (5.2) entering at $U = 294$ kph a circular cylindrical tunnel with an unvented hood when $R = 5$ cm, $R_h = 1.25R$, $\ell_h = 10R$. The open triangles ($\triangle\ \triangle\ \triangle$) are the measured pressure at a distance of 1.5 m from the hood entrance plane. The solid curve p_T is the calculated component pressure attributable to the moving source distribution representing the train; the curve p_ω is the predicted pressure generated by the vortex flows from the hood and from the tunnel; the overall predicted pressure $p_T + p_\omega$ is shown dotted (●●●).

including the influence of separation from the train, and of any large-scale vortex structures shed into the space between the train and the tunnel walls, can be treated in a similar fashion, but requires further knowledge of the flow to be useful at this stage.

For reasons discussed above in relation to approximation (5.3), it is necessary to retain only those terms in expansions (4.13) and (4.15), that correspond to waves arriving at the observer position x prior to $U[t]/R \sim 20$. In Eq. (4.13) for the pressure generated by the exterior jet, we include the terms $n = 0,\ 1,\ 2,\ 3$, which are, respectively, nonzero for $[t] > 0,\ 2\ell/c_o,\ 4\ell/c_o,\ 6\ell/c_o$ (these times are indicated in the figure). Similarly, in formula (4.15) for the pressure generated by the jet flowing from the tunnel to the hood, we can take

$$p_\omega^J([t]) \approx \frac{\rho_o U^2}{4}\mathscr{T}_J\left\{\mathrm{H}(\tau'_{-1})\left(\frac{\mathscr{A}_T(U\tau'_{-1})}{\mathscr{A}}\right)^2\left(1-\frac{2\pi\psi_J^*(R,s(\tau_{-1})-\ell_h)}{\mathscr{A}}\right)\right.$$
$$+\ (1-\mathscr{R}_J)\mathrm{H}(\tau'_1)\left(\frac{\mathscr{A}_T(U\tau'_1)}{\mathscr{A}}\right)^2\left(1-\frac{2\pi\psi_J^*(R,s(\tau_1)-\ell_h)}{\mathscr{A}}\right)$$
$$\left.-\ \mathscr{R}_J(1-\mathscr{R}_J)\mathrm{H}(\tau'_3)\left(\frac{\mathscr{A}_T(U\tau'_3)}{\mathscr{A}}\right)^2\left(1-\frac{2\pi\psi_J^*(R,s(\tau_3)-\ell_h)}{\mathscr{A}}\right)\right\}, \tag{5.4}$$

where the three terms on the right are nonzero, respectively, for

$$[t] > \ell_h/U-\ell/c_o,\quad \ell_h/U+\ell/c_o,\ \ell_h/U+3\ell/c_o,$$

as also indicated in the figure.

The plot labelled p_ω in Fig. 7 shows how the vortex generated pressure grows. The exterior jet begins to form at $[t] = 0$, and the jet flow at the junction begins at $[t] = \ell_h/U-\ell/c_o$ (i.e., $t = \ell_h/U$). The ultimate magnitude of this pressure is relatively small, however, and the corresponding increase in the overall predicted pressure rise within the compression wave (shown dotted) still falls short of the measured values at later retarded times. Nonetheless, the result indicates that the influence of flow separation and vortex generation is an important determining factor controlling the magnitude of the net pressure rise across the extended compression wavefront (prior to the entrance of the tail into the hood), and suggests that attention should be given in future studies to quantifying in more detail the properties of these secondary vortical flows.

5.4. Theory and experiment compared for model (ii)

Figs. 8 and 9 portray a corresponding accord between theory and experiment for the model train (ii) of Table 1, whose nose aspect ratio $h/L = 0.33$ is just over 50% larger than that for model (i). The experiment was performed at the higher speed of $U = 345$ kph ($M \approx 0.28$).

Because of the reduced length of the model train the last terms in each of the integrands of Eq. (5.3) do not contribute to the theoretical pressure gradient and pressure profiles shown in these figures, since the corresponding contributions arrive after the tail of the train has entered the hood (at $U[t]/R \sim 16$). The principal contributions to the waveforms are now associated with the retarded times

$$[t] = \frac{2\ell}{c_o}, \quad \frac{\ell_h}{U} - \frac{\ell}{c_o}, \quad \frac{4\ell}{c_o}, \quad \frac{\ell_h}{U} + \frac{\ell}{c_o}$$

indicated in the figures, which have the same significance as previously discussed. In particular it should be noted that, at this higher train speed the retarded times $2\ell/c_o$ and $\ell_h/U - \ell/c_o$ are closer than for model (i); the magnitude of the second peak in Fig. 8 is therefore reduced by interference with the rarefaction wave arriving at time $2\ell/c_o$. Therefore, for model (ii) the amplitude of the second peak is not substantially different from the third. The small additional

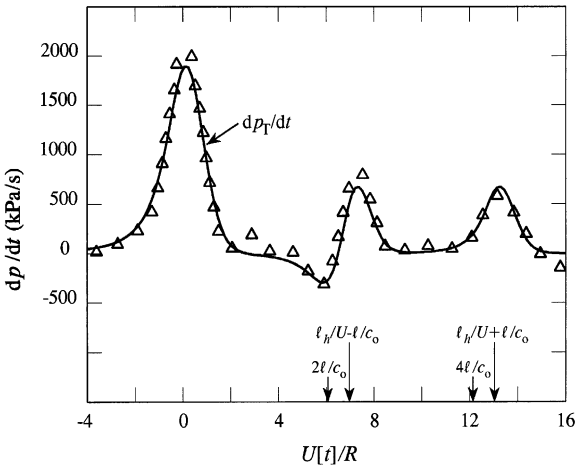

Fig. 8. The compression wave pressure gradient for train model (ii) with the ellipsoidal nose profile defined by Eq. (5.2) entering at $U = 345$ kph a circular cylindrical tunnel with an unvented hood when $R = 5$ cm, $R_h = 1.25R$, $\ell_h = 10R$. The open triangles ($\triangle\ \triangle\ \triangle$) are the measured pressure gradient at a distance of 1.5 m from the hood entrance plane. The solid curve is prediction (5.3) of the component $\partial p_T/\partial t$ of the pressure gradient attributable to the moving train alone.

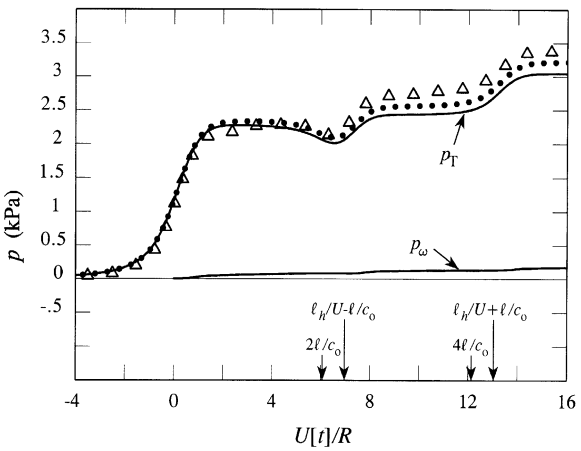

Fig. 9. The compression wave pressure for train model (ii) with the ellipsoidal nose profile defined by Eq. (5.2) entering at $U = 345$ kph a circular cylindrical tunnel with an unvented hood when $R = 5$ cm, $R_h = 1.25R$, $\ell_h = 10R$. The open triangles ($\triangle\ \triangle\ \triangle$) are the measured pressure at a distance of 1.5 m from the hood entrance plane. The solid curve p_T is the calculated component pressure attributable to the moving source distribution representing the train; the curve p_ω is the predicted pressure generated by the vortex flows from the hood and from the tunnel; the overall predicted pressure $p_T + p_\omega$ is shown dotted ($\bullet\bullet\bullet$).

contribution from the vorticity in the exit flows from the hood and tunnel have been calculated from Eq. (4.13) and (5.4); in Eq. (5.4), for example, the final term on the right-hand side makes no contribution when $U[t]/R<16$.

A comparison of Figs. 7 and 9 suggests that, as far as the overall pressure rise is concerned the agreement with experiment is better for model (ii), for the train with the shorter nose (although the difference could be a result of experimental error, at least in principle). This suggests that our neglect of separation or boundary layer growth on that section of the train within the tunnel and hood is more questionable for the longer nose (model (i)). For the short nosed train (model (ii)) the pressure rise occurs over a time interval that is too short to be affected by separation, at least during the period in which the observations are recorded.

6. Conclusion

When a high-speed train enters a long, unvented tunnel entrance hood the compression wave radiated ahead of the train into the tunnel may be ascribed to a combination of the two separate compression waves produced by the successive interactions of the train nose with the hood portal, and with the junction between the hood and tunnel. In the absence of further, secondary interactions, the total pressure rise (1.1) across the compression wave front would then occur in two separate 'steps' associated with the linear superposition of these component waves. However, a significant fraction of the energy of each component is temporarily 'trapped' within the hood by reflection from its ends; in addition the positive compression wave generated at the junction is accompanied by an expansion wave that radiates backwards over the train and is subsequently reflected at the entrance to the hood. As a result of these multiple reflections the compression wave profile in the tunnel has the following structure: A relatively large pressure rise occurs at the wave front over a distance $\sim$tunnel diameter$/M$; this corresponds to the compression wave generated as the train enters the hood. The pressure changes just to the rear of the wave front display a 'wavy' profile dominated by the compression wave generated at the junction, but greatly complicated in a well defined manner determined by the train speed and hood length, by interference between this wave and waves multiply reflected within the hood.

Our theoretical predictions of the compression wave profile, and of the pressure 'gradient' $\partial p/\partial t$, whose structure determines the amplitude of the 'micro-pressure wave' radiated from the far end of the tunnel, are based on a slender body approximation to the aerodynamic sound source that represents the moving train together with a small correction that accounts for the 'vortex sound' pressure sources in the exit flows from the hood and tunnel. An excellent correlation is obtained between observed and predicted properties of the waveforms, in particular between measured and predicted interference patterns produced because of the temporary trapping of waves in the hood. The predictions are made using a simplified Green's function for the compression wave equation that is applicable when the thickness of each of the compression wave components generated at the hood portal and at the junction is large compared to the tunnel radius. Only one portal geometry was considered in this study, but the positive overall agreement with experiment strongly suggests that our theoretical model can be used to optimize the hood dimensions to minimize the initial values of the compression wave pressure gradient. The method avoids the often cumbersome and time-consuming machine calculations involved in conventional numerical simulations of tunnel-train interactions, and yields in a matter of minutes predictions that are suitable for design studies. The results could well be used to 'benchmark' future, improved numerical schemes.

The principal uncertainty in our analysis is probably related to boundary layer development on the model trains. A growth in boundary layer displacement thickness will lead to an increase in the effective cross-sectional area $\mathscr{A}_o$ of the train, and therefore influence the magnitude of the overall pressure rise, after the train nose has entered the tunnel. Simple numerical estimates (based on laminar boundary layer theory) indicate that the maximum possible contribution from this could increase the predicted overall pressure rise across the wavefront by about 7%, or slightly less if the flow becomes turbulent during entry into the tunnel. This could well account for the differences between theory and experiment observed at large time in Figs. 7 and 9.

Typical model scale Reynolds numbers (based on train length) are estimated to be smaller than full scale by a factor $\sim 10^2$. This might suggest that boundary layer effects at full-scale are less important, although in practice the presence of protuberances on the real train means that it is not as smooth as the model, so that the contributions from boundary layer displacement at model and full-scale may well be comparable. Similarly, full-scale tunnels normally have multiple tracks, which implies that the interaction of the hood and the train will be far from axisymmetric. The main effect of this is to produce fractionally larger peaks in the pressure gradient (but no overall increase in the pressure rise, if boundary layer effects are excluded) because of a corresponding increase in the peak values of $\partial^2\varphi^*/\partial x^2$ along the track of the train.

Appendix. Green's function for a long hood

A.1. Potential flow functions for the hood

The potential functions $\varphi^*(\mathbf{x})$, $\varphi_E^*(\mathbf{x})$ and $\varphi_J^*(\mathbf{x})$ are defined in Section 3. The equivalent 'length' ℓ_j of the junction between the tunnel and hood, which occurs in definition (3.4) of $\varphi_J^*(\mathbf{x})$ is given by

$$\ell_j = \int_{-\infty}^{-\ell_h} \left(\frac{\partial \varphi_J^*}{\partial x} - 1 \right) \mathrm{d}x + \int_{-\ell_h}^{\infty} \left(\frac{\partial \varphi_J^*}{\partial x} - \frac{\mathscr{A}}{\mathscr{A}_h} \right) \mathrm{d}x, \tag{A.1}$$

where the integration is along any line within the tunnel and hood parallel to the axis of symmetry. The function $\varphi_J^*(\mathbf{x})$ varies continuously through the junction at $x = -\ell_h$, in the neighbourhood of which $\varphi_J^*(\mathbf{x}) \sim O(R_h)$. In the limit in which $\mathscr{A}/\mathscr{A}_h \to 0$ the hood is effectively replaced by an infinite flange at the tunnel entrance ($x = -\ell_h$), in which case $\ell_j \sim 0.82R$ = the 'end correction' for a flanged duct of radius R (Rayleigh, 1926).

The potential $\varphi_E^*(\mathbf{x})$, describing uniform flow from the mouth of a semi-infinite duct of radius R_h, can be cast in analytic form (Howe, 1998b), and the following particular representation is used in the numerical calculations of the main text:

$$\frac{\partial \varphi_E^*}{\partial x}(\mathbf{x}) = \frac{1}{2} - \frac{1}{2\pi} \int_0^{\infty} \mathrm{I}_0\left(\frac{\xi r}{R_h}\right) \left(\frac{2\mathrm{K}_1(\xi)}{\mathrm{I}_1(\xi)} \right)^{1/2} \sin\left\{ \xi \left(\frac{x}{R_h} + \mathscr{Z}(\xi) \right) \right\} \mathrm{d}\xi, \quad r = \sqrt{y^2 + z^2},$$

$$\mathscr{Z}(\xi) = \frac{1}{\pi} \int_0^{\infty} \ln\left(\frac{\mathrm{K}_1(\mu)\mathrm{I}_1(\mu)}{\mathrm{K}_1(\xi)\,\mathrm{I}_1(\xi)} \right) \frac{\mathrm{d}\mu}{\mu^2 - \xi^2}. \tag{A.2}$$

where I_0, I_1 and K_1 are modified Bessel functions.

A.2. The approximate Green's function

The solution of Eq. (2.4) is required at points $\mathbf{x}$ within the tunnel of Fig. 1 at distances $|x| \gg R$ from the junction with the hood; the source terms on the right-hand side are significant only within the hood or close to the ends of the hood. The corresponding Green's function for this problem can be derived by extension of the method described by Howe (1998b) for an entrance portal without a hood.

To do this we write

$$G(\mathbf{x}, \mathbf{x}'; t - \tau) = -\frac{1}{2\pi} \int_{-\infty}^{\infty} \bar{G}(\mathbf{x}, \mathbf{x}'; \omega) \mathrm{e}^{-\mathrm{i}\omega(t-\tau)}\, \mathrm{d}\omega, \tag{A.3}$$

where $\bar{G}$ satisfies the inhomogeneous Helmholtz equation $(\nabla^2 + \kappa_o^2)\bar{G} = \delta(\mathbf{x} - \mathbf{x}')$, $\kappa_o = \omega/c_o$. The characteristic frequency of the compression wave is always sufficiently small ($\kappa_o R \ll 1$) that only plane sound waves can propagate within the tunnel and hood. However, because of the area change at the junction of the hood and the uniform tunnel, multiple reflections of these waves will occur at both ends of the hood. The amplitudes of waves so trapped within the hood decrease very rapidly after two or three back-and-forth traverses of the hood as wave energy progressively radiates into the tunnel (energy losses from the mouth of the hood are negligible by comparison).

When x is large and negative (within the tunnel) the functional form of $\bar{G}(\mathbf{x}, \mathbf{x}'; \omega)$ is derived with the help of the reciprocal theorem $\bar{G}(\mathbf{x}, \mathbf{x}'; \omega) = \bar{G}(\mathbf{x}', \mathbf{x}; \omega)$ (Rayleigh, 1926), by placing the point source at $\mathbf{x}$ within the tunnel and solving for $\bar{G}(\mathbf{x}', \mathbf{x}; \omega)$ as a function of $\mathbf{x}'$ in the vicinity of the hood. At low frequencies the source generates only plane waves, and the potential of the disturbance incident on the hood from the source is equal to $\mathrm{e}^{\mathrm{i}\kappa_o(x'-x)}/2\mathrm{i}\kappa_o\mathscr{A}$ when $|x - x'| \gg R$. Thus, referring to Fig. 2, in the section T of the tunnel to the right of the source ($x' > x$), but at distances $\gg R$ from the junction J with the hood, we can write

$$\frac{\bar{G}(\mathbf{x}', \mathbf{x}; \omega)}{\Phi(x, \omega)} = \mathrm{e}^{\mathrm{i}\kappa_o x'} + \mathscr{R}_T \mathrm{e}^{-\mathrm{i}\kappa_o x'},$$

$$\text{where } \Phi(x, \omega) = \frac{\mathrm{e}^{-\mathrm{i}\kappa_o x}}{2\mathrm{i}\kappa_o \mathscr{A}}, \tag{A.4}$$

where $\mathscr{R}_T$ is a complex valued reflection coefficient. We can write down similar representations for $\bar{G}/\Phi$ for positions $\mathbf{x}'$ in the neighbourhoods of the points labelled J, H, E, and A in Fig. 2.

Because the characteristic acoustic wavelength is much larger than the tunnel and hood radii R, R_h the unsteady motion produced by the source at $\mathbf{x}$ in the vicinity of the junction J of the tunnel and hood is identical with that of an irrotational, reciprocating incompressible flow. Similarly, the flow in the mouth of the hood may be regarded as

incompressible in the leading approximation. In the mid-section H of the hood the motion will consist of plane waves of type (A.4) but with different amplitudes. Outside the hood at A, at large distances $\gg R_h$ from the mouth, the motion is that of an outward propagating spherical sound wave. The Green's function can therefore be cast in the following forms in these respective regions:

$$\frac{\bar{G}(\mathbf{x}',\mathbf{x};\omega)}{\Phi(x,\omega)} = \alpha + \beta\varphi_J^*(\mathbf{x}') \quad \text{near } J, \tag{A.5}$$

$$= \mathscr{T}_H e^{i\kappa_o x'} + \mathscr{R}_H e^{-i\kappa_o x'} \quad \text{at } H \text{ within the hood}, \tag{A.6}$$

$$= \gamma + \delta\varphi^*(\mathbf{x}') \quad \text{near } E, \tag{A.7}$$

$$= \frac{\varepsilon\, e^{i\kappa_o|\mathbf{x}'|}}{4\pi|\mathbf{x}'|} \quad \text{at } A, \tag{A.8}$$

where $\alpha,\ \beta,\ \mathscr{T}_H,\ \mathscr{R}_H,\ \gamma,\ \delta,\ \varepsilon$ depend only on the acoustic wavenumber κ_o and the dimensions of the hood and tunnel radius, and $\varphi^*,\ \varphi_J^*$ are the potential functions defined in Section 3.

The values of the coefficients $\mathscr{R}_T,\ \alpha,\ \beta,\ \mathscr{T}_H,\ \mathscr{R}_H,\ \gamma,\ \delta,\ \varepsilon$ in Eqs. (A.4)–(A.8) are related by matching the different representations of $\bar{G}/\Phi$ where neighbouring regions of validity overlap. Thus, just to the left of the junction J at $x' = -\ell_h$, where $\kappa_o|x' + \ell_h| \ll 1$ and $|x' + \ell_h| \gg R$, representations (A.4) and (A.5) must agree, i.e., making use of the first of the asymptotic forms (3.4):

$$e^{-i\kappa_o\ell_h} + \mathscr{R}_T e^{i\kappa_o\ell_h} + i\kappa_o(x' + \ell_h)(e^{-i\kappa_o\ell_h} - \mathscr{R}_T e^{i\kappa_o\ell_h}) \equiv \alpha - \beta\ell_j + \beta(x' + \ell_h),$$

and therefore

$$\begin{aligned} &e^{-i\kappa_o\ell_h} + \mathscr{R}_T e^{i\kappa_o\ell_h} = \alpha - \beta\ell_j, \\ &i\kappa_o(e^{-i\kappa_o\ell_h} - \mathscr{R}_T e^{i\kappa_o\ell_h}) = \beta. \end{aligned} \tag{A.9}$$

Similarly, by matching leading order terms, respectively, to the right of J, the left of E and in the acoustic near field of region A of Fig. 2, we find

$$\begin{aligned} &\mathscr{T}_H e^{-i\kappa_o\ell_h} + \mathscr{R}_H e^{i\kappa_o\ell_h} = \alpha, \\ &i\kappa_o(\mathscr{T}_H e^{-i\kappa_o\ell_h} - \mathscr{R}_H e^{i\kappa_o\ell_h}) = \frac{\beta\mathscr{A}}{\mathscr{A}_h}, \end{aligned} \tag{A.10}$$

$$\begin{aligned} &\mathscr{T}_H + \mathscr{R}_H = \gamma - \delta\ell', \\ &i\kappa_o(\mathscr{T}_H - \mathscr{R}_H) = \delta, \end{aligned} \tag{A.11}$$

$$\begin{aligned} &\gamma = \frac{i\kappa_o\varepsilon}{4\pi}, \\ &-\delta\mathscr{A}_h = \varepsilon. \end{aligned} \tag{A.12}$$

Eqs. (A.9)–(A.12) are sufficient to determine all of the coefficients

$$\mathscr{R}_T,\ \alpha,\ \beta,\ \mathscr{T}_H,\ \mathscr{R}_H,\ \gamma,\ \delta,\ \varepsilon.$$

The coefficient γ is $O(\kappa_o R_h) \ll 1$ relative to the smallest of all of the other coefficients; it accounts for the loss of energy by the incident wave by radiation from the mouth of the hood into free space. This loss is always negligible ($\sim O(\kappa_o^2 R_h^2)$) relative to that reflected back into the hood and tunnel when $\kappa_o R_h$ is small, and can safely be neglected (an approximation equivalent to this was made by Howe, 1998b). Representations (A.5)–(A.7) of $\bar{G}(\mathbf{x}',\mathbf{x};\omega) \equiv \bar{G}(\mathbf{x},\mathbf{x}';\omega)$ can then be cast in a common form when $\mathbf{x}'$ lies within the hood H or in the vicinities of J and E:

$$\bar{G}(\mathbf{x},\mathbf{x}';\omega) = \frac{e^{-i\kappa_o(x-\ell')}}{2i\kappa_o\mathscr{A}} \frac{(e^{i\kappa_o\varphi^*(\mathbf{x}')} - e^{-i\kappa_o\varphi^*(\mathbf{x}')})}{1+\eta}, \quad x \to -\infty, \tag{A.13}$$

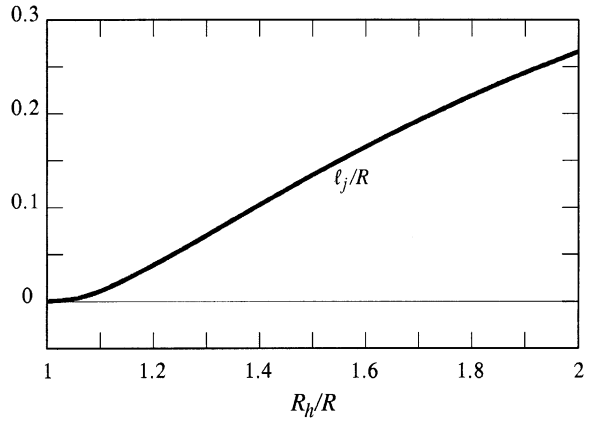

Fig. 10. Dependence of the nondimensional junction equivalent length ℓ_j/R on the ratio R_h/R of the hood and tunnel radii.

where

$$\eta = \Delta\, e^{i\kappa_o \ell} \cos(\kappa_o \ell), \quad \Delta = \frac{\mathscr{A}_h e^{-i\kappa_o \ell_j} - \mathscr{A}}{\mathscr{A}}. \tag{A.14}$$

Approximation (A.13) is uniformly valid anywhere in J, H and E; in the hood $\varphi^*(\mathbf{x}')$ can be replaced by $x' - \ell'$ to obtain representation (A.6); also, $\kappa_o \varphi^*(\mathbf{x}') \ll 1$ at E, and expansion to first order in $\kappa_o \varphi^*(\mathbf{x}')$ yields Eq. (A.7) with the free space radiation loss factor $\gamma = 0$; at J formula (3.3) is used to write $\varphi^*(\mathbf{x}')$ in terms of $\varphi_J^*(\mathbf{x}')$, whereupon representation (A.5) is recovered by expanding to first order in $\kappa_o \varphi_J^*(\mathbf{x}') \ll 1$. Furthermore, the formula remains valid when the hood *length* (as well as the radius) is compact, i.e., when $\kappa_o \ell \ll 1$, so that $\eta \to 0$ and Eq. (A.13) reduces to the formula given by Howe (1998b).

Similarly, in the tunnel region T, where $|x' + \ell_h| \gg R$, we find

$$\bar{G}(\mathbf{x}, \mathbf{x}'; \omega) = \frac{e^{-i\kappa_o x}}{2i\kappa_o \mathscr{A}} \left\{ e^{i\kappa_o x'} - e^{2i\kappa_o \ell'} \left(\frac{1+\eta^*}{1+\eta} \right) e^{-i\kappa_o x'} \right\}, \quad x \to -\infty, \tag{A.15}$$

where η^* is the complex conjugate of η.

The corresponding time-dependent forms of Green's function are obtained from Eqs. (A.13) and (A.15) by evaluation of Eq. (A.3). To obtain convenient representations suitable for application to the train entry problem we recall that in all practical cases all relevant frequencies ω can be assumed to satisfy $\kappa_o R \sim \kappa_o R_h \ll 1$. Typical values of R_h/R encountered in practice do not exceed about 1.4, and reference to Fig. 10 reveals that in these circumstances $\kappa_o \ell_j < 0.1 \kappa_o R$, and therefore that little error will be incurred by replacing Δ defined in Eq. (A.14) by

$$\Delta_o = \frac{\mathscr{A}_h - \mathscr{A}}{\mathscr{A}}. \tag{A.16}$$

Then

$$\frac{1}{1+\eta} = \frac{2}{2+\Delta_o} \left[1 + \left(\frac{\Delta_o}{2+\Delta_o} \right) e^{2i\kappa_o \ell} \right]^{-1} = \frac{\mathscr{A}\mathscr{T}_J}{\mathscr{A}_h} \sum_{n=0}^{\infty} \mathscr{R}_E^n \mathscr{R}_J^n e^{2in\kappa_o \ell}, \tag{A.17}$$

where

$\mathscr{R}_E = -1$, reflection coefficient of the open end of the hood,

$\mathscr{R}_J = \dfrac{\mathscr{A}_h - \mathscr{A}}{\mathscr{A}_h + \mathscr{A}}$, reflection coefficient of the junction end of the hood,

$$\mathscr{T}_J = \frac{2\mathscr{A}_h}{\mathscr{A}_h + \mathscr{A}}, \quad \text{transmission coefficient of the junction end of the hood.} \tag{A.18}$$

These are the limiting values of the exact reflection and transmission coefficients as $\kappa_o R \to 0$ (Lighthill, 1978). $\mathscr{R}_J$ gives the amplitude of the wave reflected back into the hood when at the junction, and $\mathscr{T}_J$ determines the amplitude of the wave transmitted from the hood into the tunnel.

Thus, using expansion (A.17) in Eq. (A.13), and evaluating the Fourier integral (A.3) we find for $\mathbf{x}'$ in J, H and E:

$$G(\mathbf{x},\mathbf{x}';t-\tau) = \frac{c_o\mathscr{T}_J}{2\mathscr{A}_h}\sum_{n=0}^{\infty}\mathscr{R}_E^n\mathscr{R}_J^n\left\{\mathrm{H}\left([t]-\tau-\frac{(2n\ell+\varphi^*(\mathbf{x}'))}{c_o}\right)+\mathscr{R}_E\mathrm{H}\left([t]-\tau-\frac{(2n\ell-\varphi^*(\mathbf{x}'))}{c_o}\right)\right\}, x\to-\infty, \tag{A.19}$$

where H is the Heaviside step function, and $[t] = t + (x-\ell')/c_o$ is the retarded time. This formula remains valid in the absence of the hood ($\mathscr{A}_h \equiv \mathscr{A}$), because $\mathscr{T}_J \to 1$, $\mathscr{R}_J \to 0$ and only the term in $n = 0$ survives, leading to the result given by Howe (1998b). For an acoustically compact hood the terms $2n\ell/c_o$ in the arguments of the Heaviside functions can be discarded, and (because $\mathscr{T}_J\sum_{n=0}^{\infty}\mathscr{R}_E^n\mathscr{R}_J^n = 1$) Eq. (A.19) then reduces to the general formula given by Howe (1999) for a compact portal of variable geometry.

A similar expansion can be derived from Eq. (A.15) for the time-domain Green's function when $\mathbf{x}'$ lies in T at distances $\gg R$ from the junction, but this is not needed in the present discussion.

References

Auvity, B., Bellenoue, M., 1998. Vortex structure generated by a train-tunnel entry near the portal. Paper presented at the Eighth International Symposium on Flow Visualization, Sorrento, Italy, 1–4 September.

Auvity, B., Bellenoue, M., Kageyama, T., 2001. Experimental study of the unsteady aerodynamic field outside a tunnel during train entry. Experiments in Fluids 30, 221–228.

Bellenoue, M., Auvity, B., Kageyama, T., 2001. Blind hood effects on the compression wave generated by a train entering a tunnel. Experimental Thermal and Fluid Science 25, 397–407.

Gregoire, R., Rety, J.M., Moriniere, V., Bellenoue, M., Kageyama, T. 1997. Experimental study (scale 1/70th) and numerical simulations of the generation of pressure waves and micro-pressure waves due to high-speed train-tunnel entry. Proceedings of the Ninth International Conference on Aerodynamics and Ventilation of Vehicle Tunnels, Aosta Valley, Italy, 6–8 October 1997. ME Publications, London, pp. 877–902.

Hara, T., 1961. Aerodynamic force acting on a high speed train at tunnel entrance. Quarterly Report of the Railway Technical Research Institute 2 (2), 5–11.

Hara, T., Kawaguti, M., Fukuchi, G., Yamamoto, A., 1968. Aerodynamics of high-speed train. Monthly Bulletin of the International Railway Congress Association XLV (2), 121–146.

Howe, M.S., 1998a. Acoustics of Fluid-Structure Interactions. Cambridge University Press, Cambridge.

Howe, M.S., 1998b. The compression wave produced by a high-speed train entering a tunnel. Proceedings of the Royal Society A 454, 1523–1534.

Howe, M.S., 1999. Review of the theory of the compression wave generated when a high-speed train enters a tunnel. Proceedings of the Institution of Mechanical Engineers Part F, Journal of Rail and Rapid Transit 213, 89–104.

Howe, M.S., Iida, M., Fukuda, T., Maeda, T., 2000. Theoretical and experimental investigation of the compression wave generated by a train entering a tunnel with a flared portal. Journal of Fluid Mechanics 425, 111–132.

Iida, M., Matsumura, T., Nakatani, K., Fukuda, T., Maeda, T., 1996. Optimum nose shape for reducing tunnel sonic boom. Institution of Mechanical Engineers Paper C514/015/96.

Ito, M., 2000. Improvement to the aerodynamic characteristics of Shinkansen rolling stock. Proceedings of the Institution of Mechanical Engineers Part F, Journal of Rail and Rapid Transit 214, 135–143.

Lamb, H., 1932. Hydrodynamics, 6th Edition. Cambridge University Press, Cambridge (reprinted 1993).

Lighthill, J., 1978. Waves in Fluids. Cambridge University Press, Cambridge.

Maeda, T., Matsumura, T., Iida, M., Nakatani, K., Uchida, K., 1993. Effect of shape of train nose on compression wave generated by train entering tunnel. In: Iguchi, M (Ed.), Proceedings of the International Conference on Speedup Technology for Railway and Maglev Vehicles, Yokohama, Japan, 22–26 November, 1993, pp. 315–319.

Matsuo, K., Aoki, T., Mashimo, S., Nakatsu, E., 1997. Entry compression wave generated by a high-speed train entering a tunnel. Proceedings of the Ninth International Conference on Aerodynamics and Ventilation of Vehicle Tunnels, Aosta Valley, Italy, 6–8 October 1997. ME Publications, London, pp. 925–934.

Milne-Thomson, L.M., 1968. Theoretical Hydrodynamics, 5th Edition. Macmillan, London.

Noble, B., 1958. Methods based on the Wiener–Hopf Technique. Pergamon Press, London.

Noguchi, Y., Okamura, Y., Uchida, K., Ishihara, T., Mashimo, S., Kageyama, M., 1996. Solving aerodynamic environmental problems arising from train speed-up. Institution of Mechanical Engineers Paper C514/039/96.

Ogawa, T., Fujii, K., 1994. Numerical simulation of compressible flows induced by a train moving into a tunnel. Computational Fluid Dynamics Journal 3, 63–82.

Ogawa, T., Fujii, K., 1997. Numerical investigation of three dimensional compressible flows induced by a train moving into a tunnel. Journal of Computers and Fluids 26, 565–585.

Ozawa, S., Tsukamoto, K., Maeda, T., 1976. Model experiments on devices to reduce pressure wave radiated from a tunnel (in Japanese). Rept. No. 990, Railway Technical Research Institute, Japanese National Railways.

Ozawa, S., Maeda, T., 1988a. Model experiment on reduction of micro-pressure wave radiated from tunnel exit. In: Emori R.I. (Ed.), Proceedings of the International Symposium on Scale Modeling, Tokyo, 18–22 July. Seikei University, Japan Society of Mechanical Engineers, pp. 33–37.

Ozawa, S., Maeda, T., 1988b. Tunnel entrance hoods for reduction of micro-pressure wave. Quarterly Report of the Railway Technical Research Institute 29 (3), 134–139.

Ozawa, S., Maeda, T., Matsumura, T., Uchida, K., Kajiyama, H., Tanemoto, K., 1991. Countermeasures to reduce micro-pressure waves radiating from exits of Shinkansen tunnels. In: Haerter, A. (Ed.), Aerodynamics and Ventilation of Vehicle Tunnels. Elsevier, Amsterdam, pp. 253–266.

Ozawa, S., Uchida, T., Maeda, T., 1978. Reduction of micro-pressure wave radiated from tunnel exit by hood at tunnel entrance. Quarterly Report of the Railway Technical Research Institute 19 (2), 77–83.

Peters, J.L., 2000. Tunnel optimized train nose shape. Paper presented at the 10th International Symposium on Aerodynamics and Ventilation of Vehicle Tunnels, Boston, USA, 1–3 November.

Rayleigh, L., 1926. The Theory of Sound, Vol. 2. Macmillan, London.

Sasoh, A., Onodera, O., Takayama, K., Kaneko, R., Matsui, Y., 1994. Experimental investigation on the reduction of railway sonic boom (in Japanese). Transactions of the Japanese Society of Mechanical Engineers B 60, 4112–4118.

Woods, W.A., Pope, C.W., 1976. Secondary aerodynamic effects in rail tunnels during vehicle entry. Paper C5. In: Stephens, H.S., Dowden, R.R., King, A.L., Patel, M.P. (Eds.), Second BHRA Symposium of the Aerodynamics and Ventilation of Vehicle Tunnels, Cambridge, England, 23–25 March 1976, pp. 71–86.

Yoon, T., Lee, S., 2001. Efficient prediction methods for the micro-pressure wave from a high-speed train entering a tunnel using the Kirchhoff formulation. Journal of the Acoustical Society of America 110, 2379–2389.